Interstitial vortex in superconducting film with periodic hole arrays



2012 Chinese Phys. B 21 087401

(http://iopscience.iop.org/1674-1056/21/8/087401)

**Rapid Communication**

# Interstitial vortex in superconducting film with periodic hole arrays*

He Shi-Kun(何世坤), Zhang Wei-Jun(张伟君), Wen Zhen-Chao(温振超), Xiao Hong(肖 宏), Han Xiu-Feng(韩秀峰), Gu Chang-Zhi(顾长志), and Qiu Xiang-Gang(邱祥冈)†

*Beijing National Laboratory for Condensed Matter Physics, Institute of Physics, Chinese Academy of Sciences, Beijing* 100190, *China*

(Received 4 March 2012; revised manuscript received 14 April 2012)

The response of superconducting Nb films with a diluted triangular and square array of holes to a perpendicular magnetic field are investigated. Due to small edge-to-edge separation of the holes, the patterned films are similar to multi-connected superconducting islands. Two regions in the magnetoresistance $R(H)$ curves can be identified according to the field intervals of the resistance minima. Moreover, in between these two regions, variation of the minima spacing was observed. Our results provide strong evidence of the coexistence of interstitial vortices in the islands and fluxoids in the holes.

**Keywords:** matching effect, interstitial vortex

**PACS:** 74.25.Ha, 74.78.Na **DOI:** 10.1088/1674-1056/21/8/087401

## 1. Introduction

Superconducting films with artificial pinning arrays of well-defined size, shape, and composition have attracted much attention in the past decade. A series of novel phenomena have been explored, including commensurate effects,[1] reconfiguration,[2] and rectification effects.[3] At the commensurate fields, vortices form ordered configurations which have the same symmetry as the underlying pinning arrays thus reduce the vortex mobility and lead to increased critical current and decreased resistance.[4] Besides, if the number of vortices trapped in the pinning sites reaches its maximum value, the extra vortices could sit at the interstitial regions between the pinning sites. If one ignores the intrinsic pinning of the film, the locations of these interstitial vortices can be determined by minimizing the interaction potential between the interstitial vortices and the trapped ones. With direct imaging experiments such as electron-beam microscopy,[5] scanning Hall probe microscopy,[6,7] and scanning tunneling microscopy,[8] the coexistence of vortices trapped in pinning sites and interstitial Abrikosov vortices has been confirmed.

However, most of these experiments were carried out at temperatures far below $T_c$, where the temperature-dependent coherence length $\xi(T) = \xi(0)/\sqrt{1-T/T_c}$ is small. At temperatures near $T_c$, transport measurements[2,9−11] have also shown that interstitial vortices can be stabilized but those works only focused on vortex arrangements with small vortex densities. The vortex configuration can be very complicated with high flux density.[8,12] Recently, it has been shown by numerical simulations that a multi-quanta interstitial vortex (giant vortex) state is favored under certain pattern geometry.[13,14] However, without direct imaging experiments, it is very difficult to determine the exact locations of the interstitial vortices.

In this work, we study the interstitial vortices up to high vortex density near $T_c$ using diluted triangular and square arrays of holes. Honeycomb and Kagomé arrays can be obtained from a triangular lattice with 1/3 and 1/4 of the sites removed, respectively.[15] In a similar way, a diluted square (DS) lattice is constructed by removing 1/4 of the sites from the original square lattice. Thus all the patterned films have large interstitial regions which allows us to investigate the behavior of the interstitial vortex. Different from previous studies,[10,15−17] the edge-to-edge separations

*Project supported by the National Basic Research Program of China (Grant Nos. 2009CB929100 and 2011CBA00107) and the National Natural Science Foundation of China (Grant Nos. 91121004, 10974241, and 11104335).

†Corresponding author. E-mail: xgqiu@iphy.ac.cn

between the holes in this work are comparable to the coherence length at the measurement temperatures. A series of local minima are observed in the magnetoresistance $R(H)$ curves. Surprisingly, the values of the field intervals between two consecutive minima vary with respect to the applied magnetic field, which is attributed to the presence of interstitial vortices. The possibility of giant interstitial vortex states in these systems is also discussed.

## 2. Experiment

The superconducting Nb films with a thickness of 60 nm are deposited by magnetron sputtering on the $SiO_2$ substrate. The micro-bridges for transport measurements were fabricated by ultraviolet photolithography and reactive ion etching. Then the desired arrays covering the whole bridge area of 60 μm × 60 μm were obtained by electron-beam lithography (EBL) on a polymethyl metacrylate (PMMA) resist layer. Finally, the patterns were transferred to the films by magnetically enhanced reactive ion etching. Figure 1 shows the atomic force micrographs of the honeycomb and the Kagomé sample on 60-nm Nb films with lattice constant $a = 400$ nm. The patterns look like thin wire connected superconducting disks.

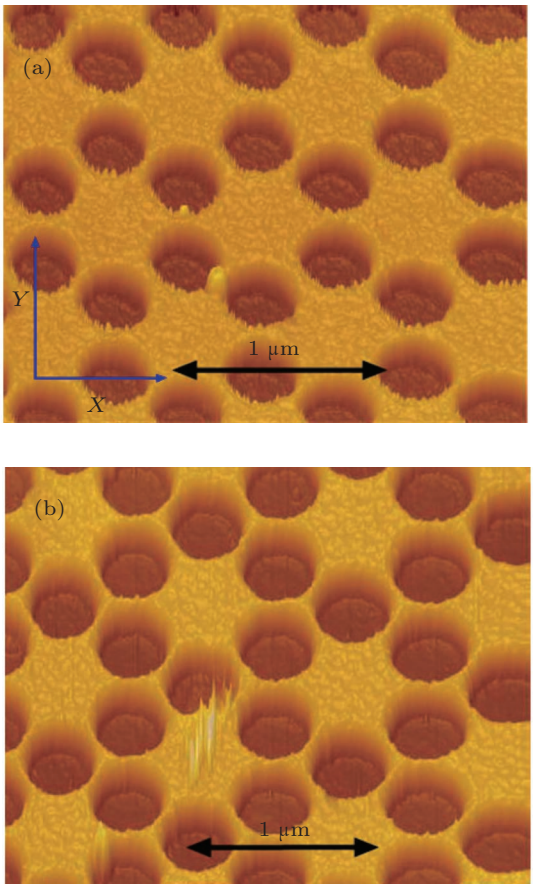


**Fig. 1.** (colour online) Atomic force micrograph (AFM) of superconducting Nb film with honeycomb (a) and Kagomé (b) array of holes. The spacing of the holes is 400 nm and the diameter is about 340 nm in (a) and 360 nm in (b).

The transport measurements were performed in a commercial Physical Properties Measurement System (PPMS) manufactured by Quantum Design. The system has a temperature stability of 2 mK during the measurements. The magnetic field was applied perpendicular to the film. The basic information of the samples is listed in Table 1. A reference film without any pattern has a higher $T_c$ of 7.65 K. The coherence length at zero temperature is $\xi(0) = 9.4$ nm according to $T_c(H)$ phase boundary measurement of the reference sample.[18] Using the dirty limit expressions $\xi(0) = 0.855\sqrt{\xi_0 l}$ and $\lambda(0) = 0.64\lambda_l\sqrt{\xi_0/l}$, where $\xi_0 = 41$ nm is the BCS coherence length[19] and $\lambda_l = 35$ nm is the London penetration depth,[20] we determined the mean free path $l = 2.95$ nm and zero temperature penetration depth $\lambda(0) = 83.5$ nm.

**Table 1.** Basic information of the samples. $D_h$ is the hole diameter, $T_c$ and $\Delta T_c$ are the superconducting transition temperature and the transition width, $R_N$ is the normal state resistance at 8 K.

| | $D_h$/nm | $T_c$/K | $\Delta T_c$/K | $R_N/\Omega$ |
|---|---|---|---|---|
| Honeycomb | $340 \pm 5$ | 7.53 | 0.18 | 28.36 |
| Kagomé | $360 \pm 5$ | 7.48 | 0.40 | 53.30 |
| DS | $360 \pm 5$ | 7.38 | 0.40 | 38.98 |

## 3. Results and discussion

Shown in Fig. 2 are the typical $R(H)$ curves measured with increasing field near $T_c$ for the diluted triangular samples. The current was applied along the $X$ axis (see Fig. 1). A set of matching minima are clearly presented, eight for honeycomb and fourteen for Kagomé. The first matching fields derived from the lattice constant are $H_1 = \Phi_0/(3/4)\sqrt{3}a^2 = 99.6$ Oe (1 Oe = 79.5775 A/m) and $H_1 = \Phi_0/(2/3)\sqrt{3}a^2 = 112.1$ Oe for honeycomb and Kagomé sample, respectively (Here $\Phi_0 = h/2e$ is the flux quantum). For detailed analysis, the field interval normalized by the first matching field $H_1$ versus the corresponding index number are shown in the insets.

First, let us concentrate on the results of the honeycomb lattice. The reduced temperature is $t = T/T_c = 0.984$. The interval between two consecutive minima is 96.3 Oe for the first three matchings which is in agreement with the theoretical value. When the field is larger than the 3rd matching field, the field spacing has a larger value of about 1.5 $H_1$, which is

very close to the matching field of the triangular lattice with the same lattice constant. We define the 4th matching field as $H_{\rm tr}$ to denote this transition. Most surprisingly, this kind of larger interval is observed twice and followed by another interval of 1.16 $H_1$ as can be seen from the inset of Fig. 2(a). After that, the field spacing of the minima equals 1.5 $H_1$ again, two clearly presented and a much weaker one near the normal phase.

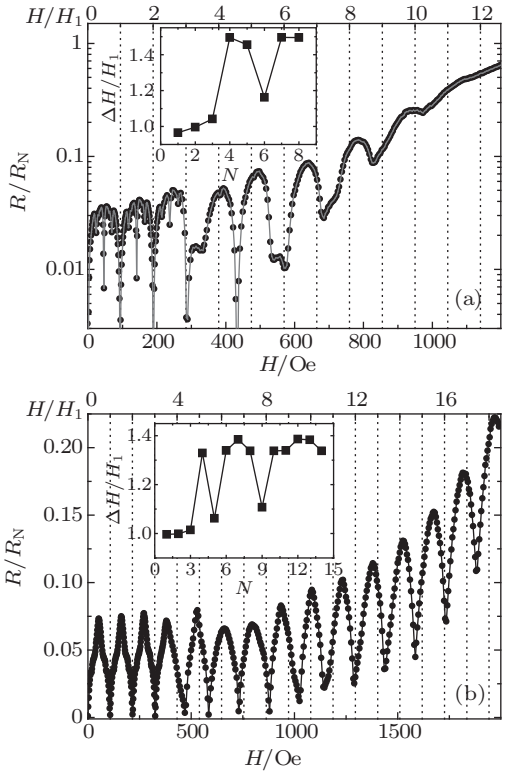


**Fig. 2.** Magnetoresistance of 60-nm Nb film with diluted triangular arrays: (a) honeycomb at $t = 0.984$, $I = 10$ μA, (b) Kagomé at $t = 0.982$, $I = 10$ μA. The resistance is normalized by the normal state resistance at 8 K. The insets show the field interval normalized by the field value of the first resistance minimum versus the index of minima.

Figure 2(b) shows the results on the Kagomé sample at $t = 0.982$. More minima are presented due to a larger hole diameter. Similar variations of the field interval are better identified. The field intervals of the first three sharp matching minima are about 108.3 Oe, again in good agreement with the predicted value. When the field is larger than the third matching, the spacing of two consecutive minima is about 1.33 $H_1$, which equals the field spacing of a triangular lattice with a lattice constant of 400 nm. Two exceptions are identified at the 5th and 9th minima, where the corresponding intervals are 1.06 $H_1$ and 1.1 $H_1$. For fields larger than the 9th matching, the intervals are all about 1.33 $H_1$ as can be seen from the inset.

Large defects with small spacing can trap vortices efficiently.[21,22] Moreover, in our samples with hole arrays, supercurrents are induced around the holes to satisfy the fluxoid quantization condition when subjected to an external field. We have recently found that in the low field region, the honeycomb and Kagomé array of holes just behave like triangular and $T_3$ wire networks, respectively.[23] When the field is small, the disk-shaped interstitial regions are in a superconducting state. No interstitial vortex is presented as illustrated in Fig. 4(a) and Fig. 4(c). Consequently, the spacial variation of the order parameter is small in a given disk and the center of the disk can be regarded as a node in a wire network. With this simplification, all the fine structures in the low field region are well described by the Alexander equations.[24]

As the field increases and reaches $H_{\rm tr}$, Abrikosov vortices are generated in the disks to minimize the Gibbs free energy. In the honeycomb and Kagomé arrays, the interstitial regions have a disk-like shape and the confinement of the periphery is significant.[25] These interstitial vortices are effectively pinned by the repulsive interactions from the fluxoids in the holes, which create a caging potential.[13] The presence of interstitial vortices results in a reconfiguration of the flux lattice from a fluxoids lattice to a composite lattice, which can be identified by the change of minima spacing in the $R(H)$ curve.[2,26] The ordered vortex arrangements just after the transition are illustrated in Fig. 4(b) and Fig. 4(d). The overall flux lattice is the interstitial vortex plus fluxoids around the holes. Here, we introduce a notation[27] $(m, n)$ to signify the configurations, where $m$ denotes the quantum number of fluxoids in one hole and $n$ denotes the total vorticity of an interstitial region. We identify different vortex configurations assuming that local dissipation minima correspond to stable vortex configurations. In an increasing field, if the minima spacing is $H_1$, the state would change from $(m, n)$ to $(m + 1, n)$. However, if the interval is $1.5H_1$ for the honeycomb or $1.33H_1$ for the Kagomé sample which equals the matching field of a triangular lattice, the state may change from $(m, n)$ to $(m + 1, n + 1)$ instead. The states corresponding to the 3rd and 4th minima in Figs. 2(a) and 2(b) are (3,0) and (4,1) respectively. Previous experimental works on a honeycomb array have found stable vortex configurations with one interstitial vortex.[10,11] Here we are able to investigate states with several interstitial vortices. However, we must note that the vortex configuration can be very complicated if several interstitial vortices are involved and we cannot determine vortex configurations in this simple way. Numerical

simulations based on the Ginzburg–Landau theory can provide useful information for determining the exact locations of the vortices.

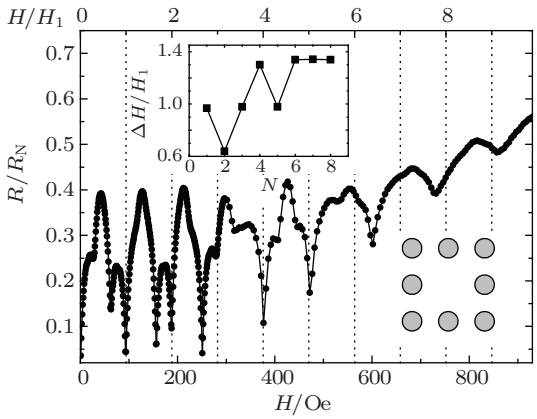


**Fig. 3.** Normalized magnetoresistance curve of a diluted square (DS) lattice at $t = 0.989$ with a current of 10 μA. The inset shows the field interval normalized by the field value of the first resistance minimum versus the minima index.

Up until now we have discussed the $R(H)$ curves of the diluted triangular lattice. In Fig. 3 we show the $R(H)$ curve of the DS sample measured at $t = 0.987$ with a current of 10 μA. The corresponding first matching field of the DS lattice is $H_1 = 3\Phi_0/4a^2 = 97$ Oe. When the field is small ($H < 5H_1$), local minima are identified at integer multiples of $H_1$. At these fields, the quantum number of the fluxoids in each hole has the same value. However, dips at fractional matching fields including 2/3, 5/3, and 8/3 are very sharp. They can be even more pronounced than the integer ones, indicating that states with an ordered fluxoids and supercurrents distribution are formed at these field values. The connectivity[24] or symmetry of the system determines these low energy states. In a honeycomb and Kagomé lattice, all the sites have the same number of nearest neighbor, which is three and four, respectively. The DS lattice, on the other hand, has two kinds of sites as can be seen from Fig. 4(e). Site A at the corner has four nearest neighbors and site B at the edge has only two. The fractional matching minima at $H = (n + 2/3)H_1$ may correspond to the states with $n + 1$ fluxoids at site B and $n$ fluxoids at site A.

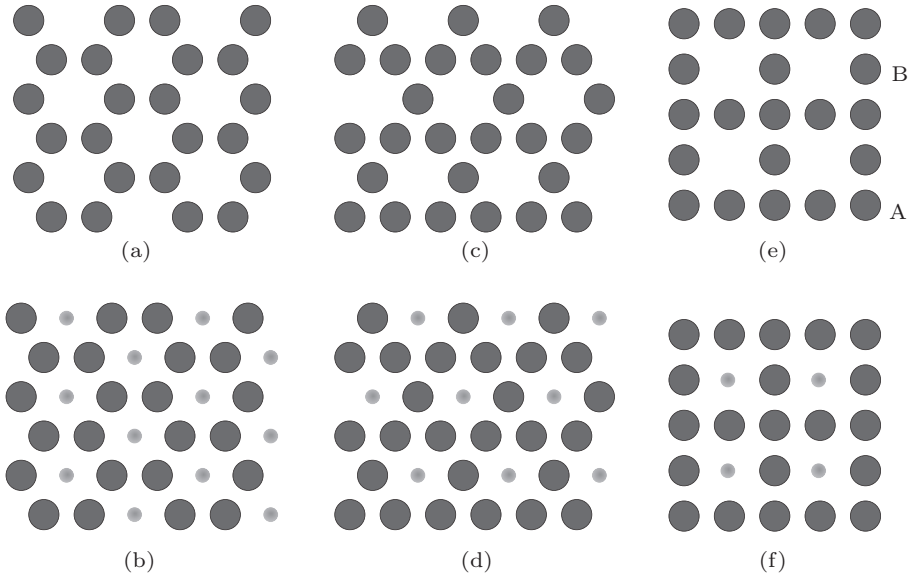


**Fig. 4.** Schematic sketch of the vortex lattice reconfiguration in honeycomb (a), (b), Kagomé (c), (d) and dilute square (DS) arrays (e), (f). No interstitial vortex states (a), (c), (e). States with one interstitial vortex at the center (b), (d), and (f). Black circles represent holes with fluxoid quanta, grey circles for interstitial vortices.

Now, let us look at the high field part of the $R(H)$ curve. For field values larger than the 5th matching, the interval between two consecutive minima is about 130 Oe. This value is very close to the matching field of the original square array which is 129.4 Oe. Similar to the observations in diluted triangular arrays, the change of the field interval is due to the nucleation of Abrikosov vortices in the interstitial region. Thus, the overall flux lattice reconfigures from the underlying DS array to square. This kind of reconfiguration is absent in a square lattice.[28] The states corresponding to the 6th minima are illustrated in Fig. 4(f). With the field further increasing, more Abrikosov vortices are generated in the interstitial sites. The confinement

of the periphery and the vortex–vortex interaction determine the locations of these vortices.

At the typical measurement temperature $t = 0.99$, the penetration depth is about 800 nm, which is even larger than the length scale of the interstitial region (about 500 nm). So the vortex generated field must overlap heavily and spacial variation of the magnetic field is negligible. The coherence length is 94 nm, which means that the vortices can still have individual cores if only a few interstitial vortices are involved. As the field increases, even the vortex cores overlap, resulting in the formation of multi-vortex states. We suggest that a giant vortex can form at the center of the interstitial region with a sufficiently high field, in agreement with simulations.[13,14] Although a giant vortex is unfavored in plain film, they can be stablized in mesoscopic disks.[25,29,30] About ten minima are observed in the high field region in Fig. 2(b). With such a high flux density, the presence of the giant interstitial vortex is possible.

## 4. Conclusions

In conclusion, magnetotransport properties of Nb films with diluted triangular and square arrays have been studied. Two regimes of the vortex lattices characterized by different intervals between two consecutive resistance minima are observed. The transition of the two regimes is due to the presence of single quantum interstitial vortices. Our findings show that these arrays can trap interstitial Abrikosov vortices effectively. Several vortices can nucleate at one interstitial site, making these systems suitable for studying the caging effect and giant interstitial vortex states.

Note added: during the preparation of this paper, the authors noticed the recent work on honeycomb arrays,[31] in which the configurations of interstitial vortices and the caging effect are studied.

## References


[1] Baert M, Metlushko V V, Jonckheere R, Moshchalkov V V and Bruynseraede Y 1995 *Phys. Rev. Lett.* **74** 3269

[2] Martin J I, Velez M, Hoffmann A, Schuller I K and Vicent J L 1999 *Phys. Rev. Lett.* **83** 1022

[3] Villegas J, Savelév S, Nori F, Gonzalez E, Anguita J, Garcia R and Vicent J 2003 *Science* **302** 1188

[4] Martin J I, Velez M, Nogues J and Schuller I K 1997 *Phys. Rev. Lett.* **79** 1929

[5] Harada K, Kamimura O, Kasai H, Matsuda T, Tonomura A and Moshchalkov V V 1996 *Science* **274** 1167

[6] Kramer R B G, Silhanek A V, Van de Vondel J, Raes B and Moshchalkov V V 2009 *Phys. Rev. Lett.* **103** 067007

[7] Grigorenko A N, Bending S J, Van Bael M J, Lange M, Moshchalkov V V, Fangohr H and de Groot P A J 2003 *Phys. Rev. Lett.* **90** 237001

[8] Karapetrov G, Fedor J, Iavarone M, Rosenmann D and Kwok W K 2005 *Phys. Rev. Lett.* **95** 167002

[9] Metlushko V, Welp U, Crabtree G W, Osgood R, Bader S D, DeLong L E, Zhang Z, Brueck S R J, Ilic B, Chung K and Hesketh P J 1999 *Phys. Rev.* B **60** R12585

[10] Wu T C, Wang J C, Horng Lance, Wu J C and Yang T J 2005 *J. Appl. Phys.* **97** 10B102

[11] Cao R, Horng L, Wu T C, Wu J C and Yang T J 2009 *J. Phys.: Condens. Matter* **21** 075705

[12] Reichhardt C J O, Libál A and Reichhardt C 2006 *Phys. Rev.* B **73** 184519

[13] Berdiyorov G R, Milosevic M V and Peeters F M 2006 *Phys. Rev. Lett.* **96** 207001

[14] Berdiyorov G R, Milošević M V and Peeters F M 2006 *Phys. Rev.* B **74** 174512

[15] Reichhardt C and Reichhardt C J O 2007 *Phys. Rev.* B **76** 064523

[16] Morgan D J and Ketterson J B 1998 *Phys. Rev. Lett.* **80** 3614

[17] Reichhardt C and Reichhardt C J O 2008 *Phys. Rev.* B **78** 224511

[18] Tinkham M 1996 *Introduction to Superconductivity* 2nd edn. (Singapore: McGraw-Hill) p. 135

[19] Weber H W, Seidl E, Laa C, Schachinger E, Prohammer M, Junod A and Eckert D 1991 *Phys. Rev.* B **44** 7585

[20] Zhang H, Lynn J W, Majkrzak C F, Satija S K, Kang J H and Wu X D 1995 *Phys. Rev.* B **52** 10395

[21] Hoffmann A, Prieto P and Schuller I K 2000 *Phys. Rev.* B **61** 6958

[22] Doria M M, de Andrade S C B and Sardella E 2000 *Physica* C: *Superconductivity* **341-348** 1199

[23] He S K, Zhang W J, Liu H F, Xue G M, Li B H, Xiao H, Wen Z C, Han X F, Zhao S P, Gu C Z and Qiu X G 2012 *J. Phys.*: *Condens. Matter* **24** 155702

[24] Alexander S 1983 *Phys. Rev.* B **27** 1541

[25] Kanda A, Baelus B J, Peeters F M, Kadowaki K and Ootuka Y 2004 *Phys. Rev. Lett.* **93** 257002

[26] Martin J I, Velez M, Hoffmann A, Schuller I K and Vicent J L 2000 *Phys. Rev.* B **62** 9110

[27] Baelus B J, Cabral L R E and Peeters F M 2004 *Phys. Rev.* B **69** 064506

[28] Kamran M, He S K, Zhang W J, Cao W H, Li B H, Kang L, Chen J, Wu P H and Qiu X G 2009 *Chin. Phys.* B **18** 4486

[29] Schweigert V A, Peeters F M and Deo P S 1998 *Phys. Rev. Lett.* **81** 2783

[30] Baelus B J, Cabral L R E and Peeters F M 2004 *Phys. Rev.* B **69** 064506

[31] Latimer M L, Berdiyorov G R, Xiao Z L, Kwok W K and Peeters F M 2012 *Phys. Rev.* B **85** 012505